Jet-Dispensing process development for a novel Nano-Ag-Sinterpaste for pressureless sintering of miniaturized opto-electronic components

Linus Daniel Stier
Fraunhofer IZM
Berlin, Germany
linus.daniel.stier@izm.fraunhofer.de

Marc Dreissigacker
Technische Universität Berlin
Berlin, Germany
marc.b.dreissigacker@tu-berlin.de

Mathias Koch
Fraunhofer IZM
Berlin, Germany
mathias.koch@izm.fraunhofer.de

Karl-Friedrich Becker
Fraunhofer IZM
Berlin, Germany
karl-friedrich.becker
@izm.fraunhofer.de

Tanja Braun
Fraunhofer IZM
Berlin, Germany
tanja.braun@izm.fraunhofer.de

Martin Schneider-Ramelow
Technische Universität Berlin
Berlin, Germany
martin.schneider-ramelow@tu-berlin.de

Adrian Stelzer
Nano-Join GmbH
Berlin, Germany
adrian.stelzer@nano-join.de

Martin Wozniak
Nano-Join GmbH
Berlin, Germany
martin.wozniak@nano-join.de

Julien Hossain
Nano-Join GmbH
Berlin, Germany
julien.hossain@nano-join.de

***Abstract*— This paper focuses on developing a contactless jetting technique to apply a novel microparticle-based silver (Ag) sinter paste suitable for pressureless sintering of miniaturized optoelectronic components. Traditional soldering methods encounter challenges at high temperatures, which can be addressed by employing advanced sintering techniques. In these techniques, the use of adapted materials plays a pivotal role in facilitating process adaptation. We detail the optimization of a contactless jet dispensing process and analyze the influence of key parameters, such as cartridge pressure, needle lift, rising time, and open time, on the precision and reliability of material deposition. We develop a volumetric flow model to characterize the jetting process, which enables fine control over the deposited dot volume and shape. Through experimental validation using square-footprint LED dice, we demonstrate a linear correlation between open time and dot volume while highlighting falling time as a free parameter affecting dot morphology. This methodology demonstrates the potential for the accurate and efficient application of sintering pastes in optoelectronic packaging and paves the way for future advancements in microelectronic assembly.**

Keywords*— *low temperature pressureless sintering, non-contact jetting, Opto-electronic systems, LED, process development

I. INTRODUCTION

In microelectronic packaging, soldering is the traditional method for forming electrical, mechanical, and thermal interconnects between dies and substrates. Soldering can be highly parallelized, making it scalable and cost-efficient. It has short processing times and high electrical and thermal conductivity. However, the advent of wide-bandgap semiconductors has led to the expectation that junction temperatures will exceed 200 °C [1]. This requires improved thermal management of packages, which traditional solder materials cannot fully provide. Consequently, the industry is shifting toward sinter connections, which offer higher thermal conductivity and electric conductivity similar to that of solder. Sinter connections also have higher melting temperatures, which eliminates the risk of remelting during board-level soldering. While significant research exists on pressure-assisted sintering of large-area components, such as dies, coolers, and heat sinks, limited research has been conducted on low-temperature, pressureless sintering (~200 °C) for small optoelectronic components [3, 4]. Achieving this requires overcoming new challenges in material research and application technologies. For example, this study moves from conventional printing and needle dispensing processes to material dosing using non-contact jet dispensing for higher-viscosity pastes. Various studies have addressed the challenges of paste dosing, typically dealing with the dosing of solder pastes and their rheological behavior [5, 6, 7], as well as, more recently, the dosing of liquid metal [8]. Herein, we present a model that precisely controls the volume and shape of the applied depots using contactless jet dispensing. Furthermore, we evaluate the performance and reliability of a newly developed, low-temperature, pressureless Ag sintering paste that, unlike typical sintering pastes, is suitable for jet dispensing.

II. MODELLING

A. Material:Silver-Sintering Paste

The silver sintering paste used in this study was provided by Nano-Join GmbH, a German manufacturer of sintering pastes located in Berlin. This material is under development and aims to achieve reliable sinter interconnects in a pressure-less sintering process while ensuring fine dispensability. The paste system, which is stable at room temperature, has been redesigned entirely for the intended application. It contains special silver microparticles measuring less than 10 µm, combined with silver metal organics and an innovative binder system. This allows for the formation of dense, void-free, and reliable sintered interconnects. To achieve the desired pressureless process with reproducible parameters, we chose to use a convection oven with a significantly reduced sintering temperature of 200°C in air or nitrogen. This low peak temperature favors many optoelectronic components and meets the industry's demand for lower process temperatures [9]. To better understand the paste's behavior during jetting and to find the ideal processing conditions, we characterized the paste rheologically, as shown in Figure 1. The analysis shows a slight decrease in viscosity up to 30 °C; then, it slowly increases, possibly due to the evaporation of

volatile components. This limits the upper bound of the processing temperature during jetting to 30 °C.
Additionally, the ductile Ag particles increase the risk of interlocking and agglomeration, which can lead to nozzle clogging during jetting due to high forces and shear rates. To overcome these challenges, the equipment and process parameters must be adjusted to achieve stable, reliable jet dispensing.

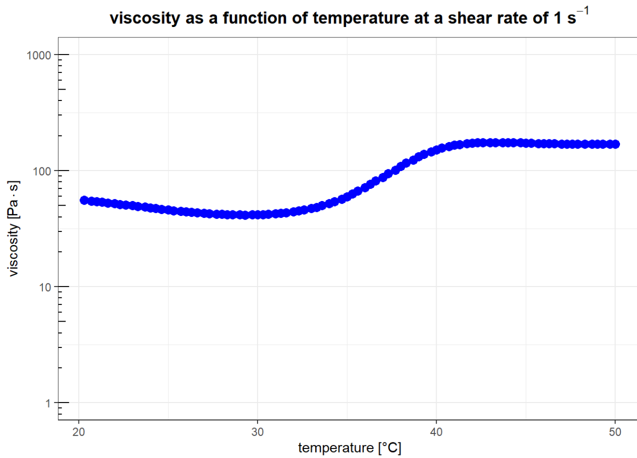

Figure 1: Viscosity vs. Temperature at shear rate $\dot{\gamma} = 1\ s^{-1}$

B. Process: Jet-dispensing

In this work jet-dispensing is done using a Vermes MDV 5100-NB piezoelectric jetting valve mounted on an Infotech FC1200 manufacturing cell as shown in Figure 2 (left).

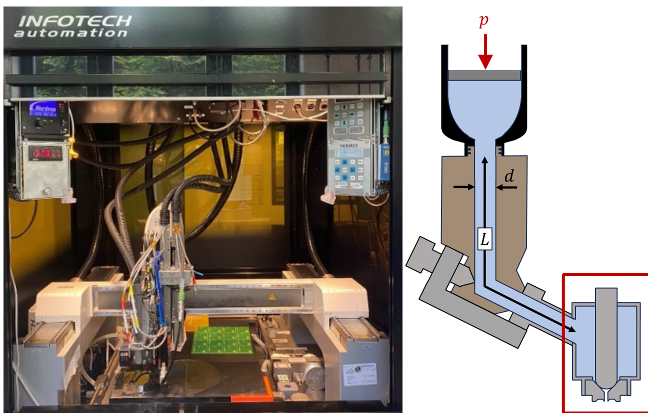

Figure 2: Infotech FC1200 with Vermes MDV 5100-NB jetting valve (left); schematic sketch of fluidic module (right)

Figure 2 (right) shows the jetting valve, which consists of the valve itself and a fluidic module that houses the tappet and nozzle. The fluidic module conveys the paste-like material from the pressurized cartridge to the nozzle chamber, which contains the nozzle and tappet. Nozzles and tappets are available in various shapes and sizes, each designed for dispensing different materials. For this study, we used an N11 250 nozzle (a 90° tapered carbide cone with a 250 µm opening) paired with a TTF-15 tappet (a cylindrical tappet with a 1.5 mm spherical carbide tip) in Section III, and an N64 120 nozzle (a 60° tapered carbide cone with a 120 µm opening) paired with an SNTF-6 tappet (a cylindrical tappet with a 1.5 mm spherical ceramic tip) in Section IV. The nozzle size was selected to be as small as possible to dispense the smallest droplets while being large enough to prevent clogging. The tappet was chosen to be compatible with the nozzle and as small as possible to jet-dispense the smallest droplets.

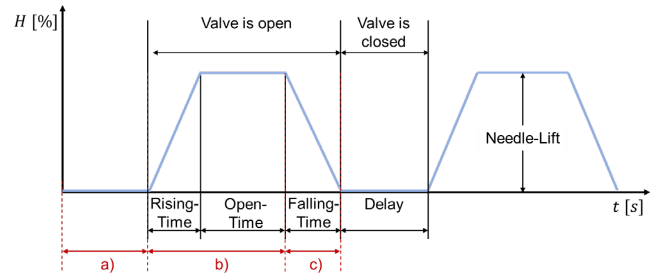

Figure 3: Tappet movement during jetting-process

The jet-dispensing process is primarily characterized by the tappet's movement over time (see Figures 3 and 4), which is controlled by a piezoelectric drive. The process can be divided into three main stages. In stage A, the tappet is not displaced, sealing the nozzle outlet (needle-lift H = 0%). In stage b), the tappet displaces by the set needle-lift value (H), opening the nozzle. The time it takes to reach this value is called the rising time (t_r). In stage c), the tappet remains displaced for the open time (t_o), enabling material to flow into the nozzle chamber. Rising time and open time are key parameters that determine the dot volume because longer times allow more material to flow into the nozzle chamber. The other two parameters are cartridge pressure, which adjusts the volume flow, and needle lift. Cartridge pressure determines the pressure at the valve, which affects volume flow. Meanwhile, maximum needle lift strongly influences maximum dot volume. During the falling time (t_f), the tappet moves back down to its initial position, ejecting the sinter paste. Consequently, a shorter falling time results in higher kinetic energy being applied to the material, thereby increasing the velocity of the ejected material. Controlling the amount of kinetic energy applied to materials with ductile fillers is crucial, as high kinetic energy increases the risk of particle agglomeration and nozzle clogging.

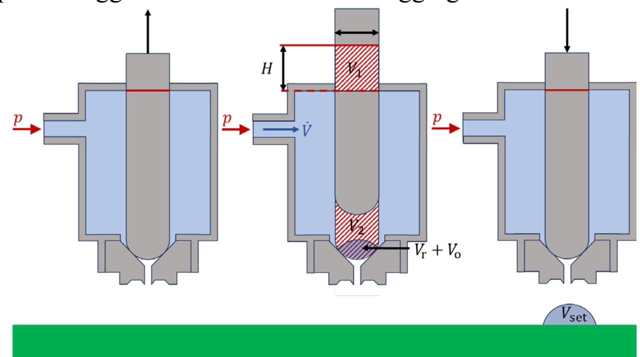

Figure 4: Schematic of jetting procedure

For a deeper understanding of the process and its parameters, we propose to model volumetric flow in the fluidic channel using the *Hagen-Poiseuille-Equation* (1). It is derived from the *Navier-Stokes-Equations* for stationary laminar flow of an incompressible Newtonian fluid in a constant diameter pipe, assuming no slip conditions at the boundary (i.e. inner surface of the modeled fludic channel. Here, $\dot{V}$ is the volumetric flow

rate, Δp is the pressure applied at the cartridge, η is the material's dynamic viscosity, $r = 1.25$ mm the radius and L = 55 mm the length of the fluidic channel.

$$\dot{V} = \frac{\pi \cdot r^4 \cdot \Delta p}{8 \cdot \eta \cdot L} \quad (1)$$

To obtain the right parameter set needed for a specific dot volume it is necessary to know the volume released by moving the tappet to its set needle-lift $V_1 = V_2 = V$ value as it limits the maximum dot volume (see Figure 4). This can be obtained using (2).

$$V = \frac{H \cdot h \cdot \pi \cdot d}{400} \quad (2)$$

Here H (in %) is the needle-lift, $h = 330$ µm is the maximum tappet travel distance and d is the tappets diameter ($d = 1.5$ mm for TTF-15 and $d = 0.6$ mm for the SNTF-6 tappet). The lower dot volume limit V_r is set by the lowest configurable rising-time, as material flows into the nozzle-chamber once the tappet is displaced. This volume is given by (3).

$$V_r = \dot{V} \cdot t_r \quad (3)$$

The volume to be filled during the open-time V_o to eject V_{set} is determined by (4).

$$V_o = V_{set} - V_r \quad (4)$$

Using this, it is possible to determine the open-time t_o needed for jetting the desired dot volume V_{set} as shown in (5).

$$t_o = \frac{V_o}{\dot{V}} \quad (5)$$

Utilizing this, (theoretical) target open-time, cartridge pressure and needle-lift as main parameters influencing dot volume, were calculated. Conveniently, falling-time remains a free parameter, which will be used to adjust the diameter of the jetted depot.

III. Validation of Process Model

To validate the influence of the parameters outlined in Section II.B, we employed two experimental groups to develop an approach for determining the optimal parameter set for a given application. In this case, we optimized square-footprint LED dice with an edge length of 980 µm and a height of 190 µm. We determine the target volume and, based on that, calculate the target volume of the jetted depot because the volume of the sintering paste decreases by approximately 58% when sintered. According to common practice, the adhesive (in this case, sintering paste) should wet no more than two-thirds of the chip height. Using the formula for the volume of a frustum of a pyramid and subtracting the chip volume, we calculated a wet target volume of $V_{wet} = 7{,}19 \cdot 10^7$ µm^3.

A. Experimental Group 1 (EG1)

In the first group we measured the dot volume at various open-times and pressures with needle-lifts of $H = 80$ % and $H = 70$ %. We obtained the dot volume values by jetting five sets of 100 dots each and measuring their weight for each data point. Using the material's density, we calculated the mean dot volume of a single droplet. The results are shown in Figure 5 ($H = 80$ %) and Figure 6 ($H = 70$ %). For this experiment the rising-time is set to its lowest possible value, while the falling-time was adjusted to ensure no material residues were left under the nozzle. This resulted in the parameter sets shown in Table 1, resulting dot volume vs open time for both needle lift setting is shown in Figure 5 and Figure 6.

Table 1: Parameter sets for EG1

H in [%]	t_r in [ms]	t_f in [ms]	T in [°C]
80	0.21	0.35	30
70	0.24	0.40	30

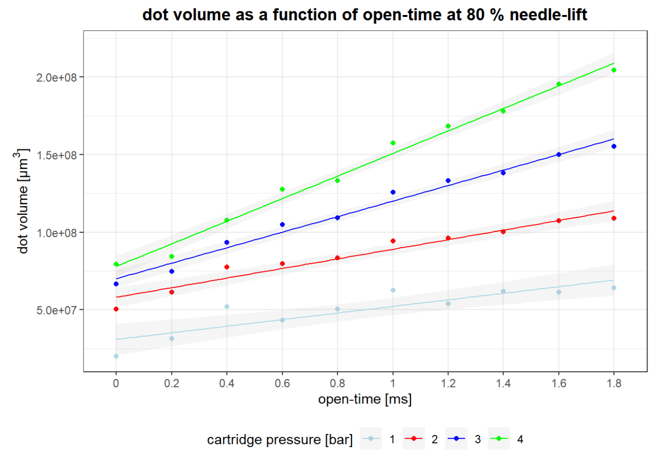

Figure 5: Dot volume as a function of open-time at 80 % needle-lift

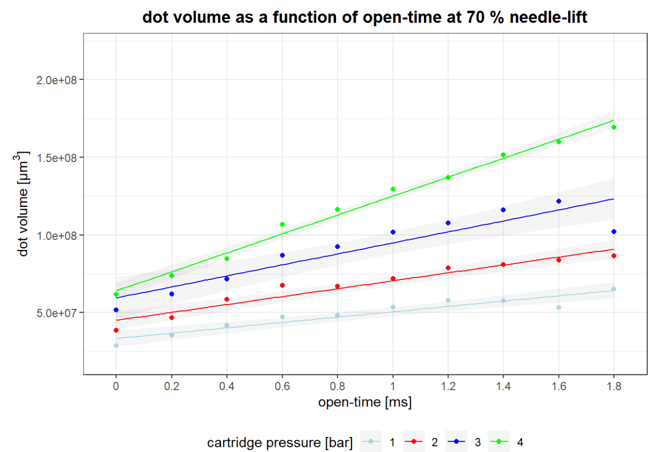

Figure 6: Dot volume as a function of open-time at 70 % needle-lift

The dot volume shows a linear correlation with open-time and cartridge pressure. Comparing Figure 5 and Figure 6, a higher needle lift also yields an increased dot volume. Additionally, it becomes clear that, multiple parameter sets can achieve the same droplet volume. Regarding the application example we selected a parameter set that provides a dot volume of $V_{wet} = 7.17 \cdot 10^7$ µm^3 which is 0.34 % smaller than the target volume for assembling the 980 µm LED. The parameter set is shown in Table 2 and will be further optimized in III.B regarding its falling-time.

B. Experimental Group 2 (EG2)

In EG1, all parameters directly influencing dot volume were examined. Leaving the falling-time as the only unexamined parameter, it is investigated further in EG2. Therefore, all other parameters were fixed according to III.A (shown in Table 2) and falling-time is varied between 0.1 ms and 0.3 ms to determine its influence on the dot, conducting high-speed recordings, microscopic imaging and measurements of volume and radius.

Table 2: Parameter set for EG2

H **in [%]**	***T*** **in [°C]**	***p*** **in [bar]**	t_r **in [ms]**	t_o **in [ms]**	t_f **in [ms]**
70	30	3	0.21	0.4	0.1…0.3

When comparing the droplet detachment at different falling-times in Table 3 using high-speed imaging, it can be seen that longer falling-time results in material being ejected more slowly [as seen in 1) in Table 3]. Also, shorter falling-times results in the material spreading thinner over a larger area [comparing 2) and 5)]. Moreover, shorter falling-times seem to move the pinching point nearer to the nozzle leaving less material under the nozzle which leads to less material being withdrawn back into the nozzle. At a falling-time of 0.3 ms the tappet's momentum is too low, leaving material under the nozzle [comparing 5)], which excludes 0.3 ms for the following experiments.

Table 3: High speed camera imaging of droplet detachment at different falling-times

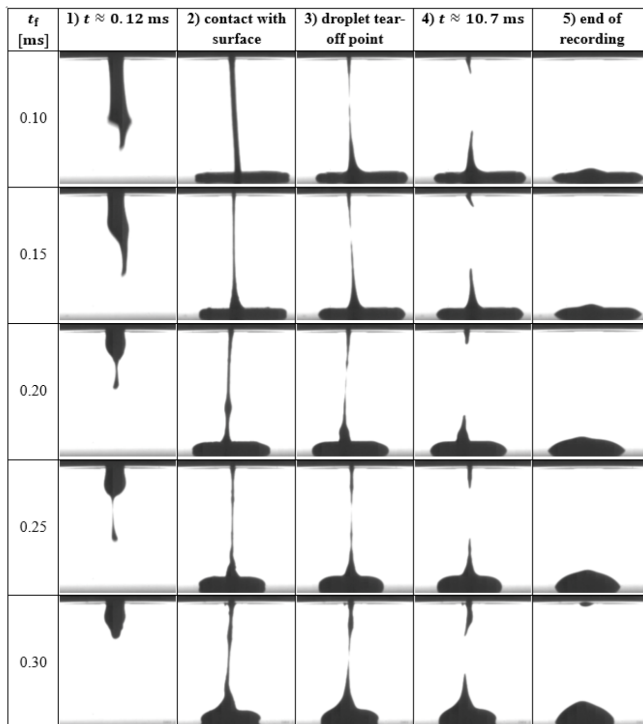

The insights found conducting high-speed recordings are reflected in the measurement of dot volume and dot radius over falling-time when jetting 1024 dots per examined falling-time. The dot volume is nearly constant over the examined falling-times, as shown in Figure 7. The dot radius decreases with increasing falling-time, as is shown in Figure 8. This indicates that the falling-time primarily affects the shape of the jetted dots, influencing their radius and height, rather than their volume. For jetting materials containing ductile fillers, increasing the falling-time minimizes the kinetic energy applied to the material which may lower the risk for nozzle clogging from particle agglomeration.

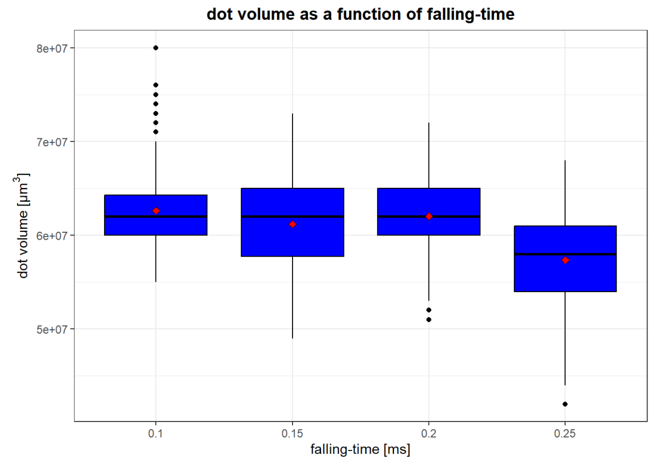

Figure 7: Dot volume as a function of falling-time

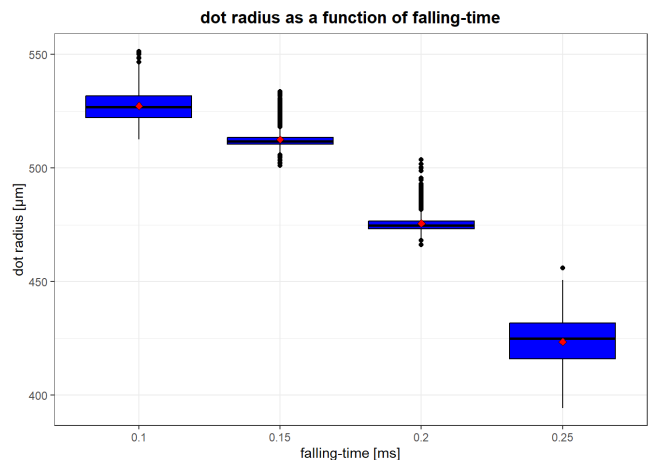

Figure 8: Dot radius as a function of falling-time

Regarding the sample application we selected a falling-time of $t_f = 0.2$ ms for assembling the 980 µm LEDs as the standard derivation is minimal for dot volume and the second smallest for dot radius (see Table 4). Additionally, the dot radius is roughly half the size of 980 µm LED. Moreover, there are no missing dots nor satellites when jetting 1024 dots (see Figure 9, left) indicating a stable process.

Table 4: Mean value and standard derivation of dot volume and radius when varying falling-time

t_f **in [ms]**	**Average dot volume in [µm³]**	**Average dot radius in [µm]**
0.10	$6.26 \cdot 10^7 \pm 3.44 \cdot 10^6$	527.30±6.84
0.15	$6.12 \cdot 10^7 \pm 4.93 \cdot 10^6$	512.53±4.17
0.20	$6.20 \cdot 10^7 \pm 3.44 \cdot 10^6$	475.61±4.20
0.25	$5.74 \cdot 10^7 \pm 4.75 \cdot 10^6$	423.51±10.93

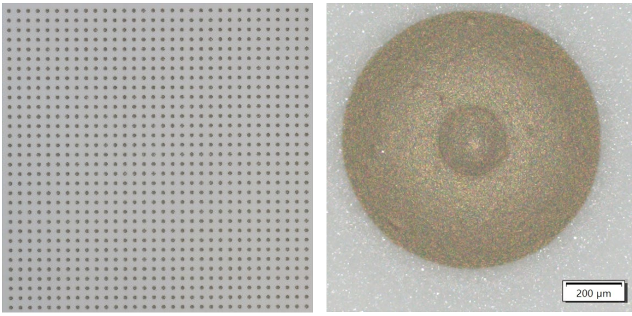

Figure 9: 1024 jetted dots at $t_f = 0.2\ ms$; overview (left), detail (right)

C. Demonstration

Concluding the validation of the process model, we assembled five 980 µm LEDs on a DCB with the parameter set found in the preceding sections. As shown in Figure 10 the determined parameter set yields the correct dot volume for contacting the LEDs.

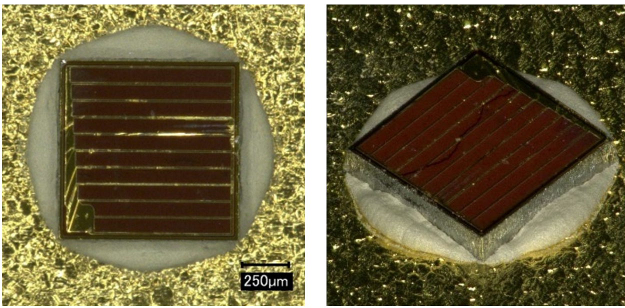

Figure 10: LED after placement

When measuring the mean wet dot volume $V_{\mathrm{D,w}} = 7.06 \cdot 10^7 \mu\mathrm{m}^3$ it is 1.8 % smaller than the target volume. Moreover, the mean sintered volume is 5.6% greater than the target sintered volume, yielding $V_{\mathrm{D,s}} = 3.19 \cdot 10^7 \mu\mathrm{m}^3$. Additionally, the average bondline thickness is 14 µm after placement and 8 µm after sintering.

IV. Assessment

In this section we analyze the sintering pastes reliability through shear tests. After assembling 980 µm LEDs in III.C we move on to smaller LEDs of 313 µm, as we target smallest depot volumes and hence smallest components. We compare their shear strength when sintered under air and nitrogen. To assess long-term reliability, we conducted temperature cycling (TCT) and high-temperature storage tests (HTS) comparing the results with initial samples. TCT cycling was done between -55°C and 125°C for 250, 500, and 1000 cycles. HTS was performed at 200°C for 250, 500 and 1000 hours. An overview for all samples is given in table Table 5.

Table 5: Overview for all samples

DCB Nr.	**LED**		**Sintering**		**Condition**
	Size in [µm]	***Number***	***Temperature in [°C]***	***Atmosphere***	
1	313	10	200	Air	Initial
2	313	10	200	N_2	Initial
3	313	15	200	Air	TCT
4	313	15	200	N_2	TCT
5	313	15	200	Air	HTS
6	313	15	200	N_2	HTS

A. Assembly of samples

For assembling the 313 µm LEDs, first we determined the necessary dot volume and identified the parameter set required to achieve this, using the approach developed under III. Therefore, we jetted a single droplet on a DCB with a diameter of ~385 µm, as shown in Figure 11 (left).

After jetting, the LEDs are placed using a manual fineplacer equipped with a specifically designed and manufactured placement tool setting the bondline thickness to 20 µm. The LEDs are then sintered at 200 °C for 2 hours, as shown in Figure 11 (right), with one half sintered in an air atmosphere and the other half in a nitrogen atmosphere.

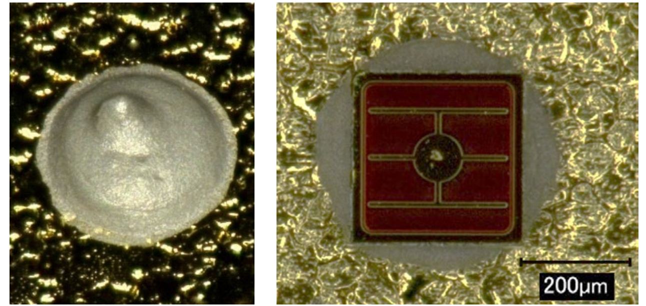

Figure 11: Sintered (left) and 313 µm LED (right) sintered

B. Shear tests

All LEDs were sheared at room temperature using a Dage 4000 bond tester equipped with a BS 5 kg cartridge and a SHEAR-187-050 chisel. The test speed was set to 300 µm/s with the shear height set to 100 µm.

The results of the temperature-cycling tests are shown in Figure 12, while the results of the high-temperature storage tests are presented in Figure 13. Hereby only the shear-test results are included where the sintered interface failed. From the initial 20 values, 12 were included. For temperature cycling tests, 16 of 30 were included, and for high-temperature storage tests, 23 of 30 values were included. Both tests show a higher die-shear strength for LEDs sintered in a nitrogen atmosphere, excluding 500 cycles TCT. Initially the die-shear strength is ~44 MPa when sintered in air atmosphere and ~54 MPa when sintered in N_2-atmosphere. Also, there is no significant decrease in die-shear strength after 1000 cycles as well as after 1000 hours at 200°C (see Table 6), pointing towards promising long-term reliability potential of the novel sintering paste formulation.

Table 6: Average die-shear strength at 1000 cycles (-50°C…125°C) and 1000 h at 200°C

Average die-shear strength in [MPa]					
Initial		***1000 cycles (-50°C…125°C)***		***1000 h at 200°C***	
Air	*N_2*	*Air*	*N_2*	*Air*	*N_2*
44.18 ±1.24	53.99 ±8.71	53.05 (n=1)	54.63 ±4.80	61.74 ±7.04	64.96 ±5.00

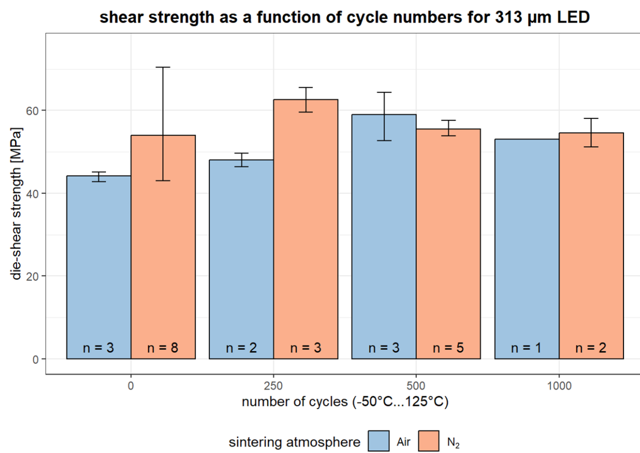

Figure 12: Die-shear strength over number of cycles (-50 °C…125 °C)

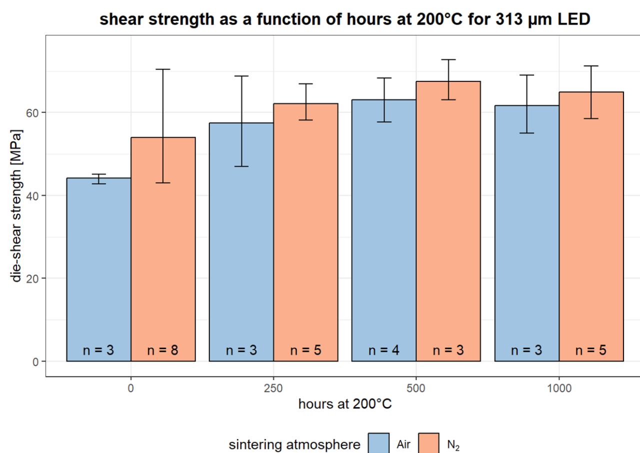

Figure 13: Die-shear strength over hours at 200 °C

C. Conclusion

The present work explores methods for jet dispensing pressureless silver sintering paste. A developmental formulation of Nano Join GmbH's nano-Ag sinter paste is used for method and process development. The paste is characterized rheologically in Section II.A, which determines the maximum jetting temperature. Next, the jet-dispensing process is examined in depth in Section II.B, and a volumetric model is created to highlight the influence of different parameters on the jetted dot. Cartridge pressure, needle lift, rise time, and open time were found to directly impact the volume of material jetted, leaving falling time as a free, volume-neutral parameter.

These insights were validated in Section III by employing two experimental groups and establishing a method for identifying the ideal parameter set for a specific application, as demonstrated with 980 µm LEDs. III.A reveals a linear interrelationship between open time and dot volume. III.B confirms that falling time is a volume-neutral parameter that influences the shape of the jetted dots in terms of both radius and height.

In Section IV, the method for identifying the optimal parameter set is applied to assemble 313 µm LEDs, showcasing the method's universality. Long-term reliability assessments were performed using temperature cycling tests and high-temperature storage. Die-shear strengths for sintering in air and nitrogen atmospheres were compared, showing higher shear strength when sintered in nitrogen. Initially, the average shear strength is ~44 MPa in air and ~54 MPa in nitrogen. Furthermore, no decrease in die shear strength was observed for either temperature cycling or high-temperature storage. After 1,000 cycles ranging from -50°C to 125°C, the average shear strength was ~53 MPa for air and ~54.6 MPa for nitrogen. Additionally, the average shear strength after 1,000 hours at 200 °C is ~61.7 MPa for air and ~65 MPa for nitrogen.

In summary, we present a straightforward methodology for accurately forming dots of a desired volume, allowing to adjust the diameter using the falling time of the tappet as a free parameter. We successfully mitigate well-known issues of particle agglomeration and nozzle clogging, paving the way for jet-dispensing of materials with ductile particles – such as NanoJoin's novel Ag sinter paste – for small components, i.e. for optoelectronic applications.

Acknowledgment

Parts of this work were performed within the project NanoLite funded by the German Federal Ministry for Economic Affairs and Climate Action (Bundesministerium für Wirtschaft und Klimaschutz, BMWK) within the ZIM-program (Zentrales Innovationsprogramm Mittelstand) under grant No. KK5076118AG1.

References

[1] „Silver Sintering vs Soldering in High Power Density Power Electronics Circuits“, Rogers Corporation Blog., Available: https://rogerscorp.com/blog/2017/silver-sintering-vs-soldering-in-high-power-density-power-electronics-circuits

[2] L. Braunwarth, S. Amrhein, T. Schreck, M. Kaloudis; Ecological comparison of soldering and sintering as die-attach technologies in power electronics, Journal of Cleaner Production, Volume 102, 2015, Pages 408-417, ISSN 0959-6526.

[3] H. Zhang, K. Suganuma, (2019). Sintered Silver for LED Applications. In: Siow, K. (eds) Die-Attach Materials for High Temperature Applications in Microelectronics Packaging. Springer, Cham.

[4] B. Rábay, A. Stelzer; Silver-Copper mixed paste for application in Die- and substrate attach; Proc. Mikrosystemtechnik-Kongress 2023, Ludwigsburg, Germany.

[5] K.-F. Becker, M. Koch, S. Voges, T. Thomas, M. Fliess, J. Bauer, T. Braun, R. Aschenbrenner, M. Schneider-Ramelow, K.-D. Lang; Precision Jetting of Solder Paste – A Versatile Tool for Small Volume Production; Proc. IMAPS International 2014, San Diego, Ca, USA.

[6] A. Pietrikova, M. Kravcik; Investigation of rheology behavior of solder paste; Proc. 35th Int. Spring Seminar on Electronics Technology, IEEE 2012, pp. 138-143

[7] S. Mallik, N.N. Ekere, A.E. Marks, A. Seman, R. Durairaj; Modelling of the time-dependent flow behavior of lead-free solder pastes used for flip-chip assembly applications; Proc. 2nd ESTC 2008, Greenwich, UK, pp. 1219-1224

[8] J. Maslik, G. Mårtensson, A. Gumiero, E. Cometti and K. Hjort, "Development of a Non-Contact Jet Dispensing of Liquid Metals," *2024 IMAPS Nordic Conference on Microelectronics Packaging (NordPac)*, Tampere, Finland, 2024, pp. 1-6, doi: 10.23919/NordPac61094.2024.10582270.

[9] H. Zhang, G. Zou, L. Liu, A. Wu and Y. N. Zhou, "Low temperature sintering of silver nanoparticle paste for electronic packaging," *2016 International Conference on Electronics Packaging (ICEP)*, Sapporo, 2016, pp. 314-317